Larhyss Journal, ISSN 1112-3680, n°55, Sept 2023, pp. 191-213

THE 2A TRIANGULAR WEIR DESIGN, THEORY, AND EXPERIMENT

ACHOUR B.[1], AMARA L.[2]

[1] Professor, Research laboratory in subterranean and surface hydraulics (LARHYSS), University of Biskra, Algeria.
[2] Associate Professor, Department of Civil Engineering and Hydraulics, LGCE Laboratory, University of Jijel, Ouled Aissa, Jijel, Algeria.

(*) bachir.achour@larhyss.net

Research Paper – Available at http://larhyss.net/ojs/index.php/larhyss/index
Received March 12, 2023, Received in revised form August 6, 2023, Accepted August 10, 2023

ABSTRACT

The 2A triangular weir is a new type of weir that belongs to the category of weirs with a triangular longitudinal profile. The current device has the same upstream and downstream slopes as the Crump weir. The study intends to derive the theoretical relationship that governs the discharge coefficient C_d of the device and hence that of the flow rate Q, known as the stage-discharge relationship. For this, the energy equation, involving the approach flow velocity, is applied between two judiciously chosen sections of the free flow crossing the weir under critical state conditions. The resulting equation is transformed into dimensionless terms, and the discharge coefficient is derived by comparison with the well-known stage-discharge relationship of triangular weirs. Another method, based on the kinetic factor, is also applied and leads to the same result. The theoretical discharge coefficient relationship shows that only the relative weir height is the influential parameter, as predicted by the dimensional analysis. The shape of the approach channel has no influence either on the discharge coefficient C_d or on the flow rate Q. This feature gives the device a universal range since its use can be extended to any shape of the approach channel.

Keywords: Novel type weir, 2A weir, Stage-discharge relationship, Discharge coefficient, Experimental validation.

INTRODUCTION

The category of weirs with a triangular longitudinal profile includes the universally known weirs of Crump and Bazin (Bazin, 1898; Henderson, 1966; Bos, 1976; 1989; Hager, 1986). They are formed of rectangular cross-sections and have an upstream face

and a downstream face, with given slopes. While Bazin adopted four combinations of upstream and downstream slopes, Crump limited the structure to a single combination, i.e., 1:2 upstream and 1:5 downstream. The few studies carried out on the Crump weir have confirmed that these slope values are adequate such that no separation of the liquid nappe above or downstream of the weir crest has been observed for a wide range of discharge (Filippov and Brakeni, 2007; Zuikov, 2017), meaning that a clinging nappe is formed having no air beneath and the streams flow along the downstream face of the weir.

Made up of rectangular cross-sections, the Crump- and Bazin-type weirs are not a universal range since their use is restricted to the rectangular open channel. Furthermore, the Bazin weir did not experience the desired attractiveness because it was calibrated for a crest height P = 50 cm, which is too large a crest height for existing practical installations (Afblb, 1970). Since then, no study has been carried out to correct this drawback.

It is well known that rectangular sections have many disadvantages when used as a measuring structure (Kindsvater and Carter, 1957; Kulin and Compton, 1975). The discharge coefficient C_d is not actually a constant for a given installation but is a function of the flow depth h above the rectangular weir crest. The main reason is that the ratio of h to the wetted perimeter p of the crest is not constant since h/p is a function of the aspect ratio b/h, where b is the crest width, which is also the width B of the approach channel in the case of a suppressed weir (Thomson, 1861; SIA; 1926). In contrast, in the case of a V-notch, the ratio h/p is actually a constant for a given installation since it solely depends on the vertex angle (De Coursey and Blanchard, 1970; Kulin and Compton, 1975; Shen, 1981; Boiten and Pitlo, 1982). As a result, the discharge coefficient C_d of such a structure does not depend on the relative depth h/B, provided that no transition is made between the measurement structure and the approach channel. If a transition is operated, particularly if it is abrupt, then in this case, the discharge coefficient C_d depends on the dimensionless parameter mh/B, where m is the tangent of the half vertex angle (Thomson, 1861; Shen, 1981; USBR, 1997; Achour and Amara, 2022a; Nicosia and Ferro, 2022).

Additionally, for low flow rates, the rectangular section resulted in shallow depths h, thus causing appreciable depth reading errors, while the V-notch causes great depths h, which can be gauged with high accuracy. Hence, depth measurement can be performed more accurately over the triangular weir than over the rectangular weir, which implies a better accuracy in the flow rate computation using the stage-discharge relationship. Whether for low or high flows, the relative error caused by the depth h reading is the same when the triangular section is used as the measurement structure. This is because the triangular section offers perfect geometric similarity.

Keeping in mind the advantages offered by the triangular section as a measuring structure, the authors recommend a new type of weir with a triangular longitudinal profile made up of triangular cross sections, which is expected to be as efficient as it is accurate. Its design has been carefully studied, as will be described in the next section, to give the measurement structure a universal range. Unlike most devices, the recommended weir is in fact not connected to the approach channel walls by a transition, so it can be used in

any form of approach channel without affecting the governing stage-discharge relationship.

What is expected from the study is to derive the governing discharge coefficient C_d relationship of the weir using an irreproachable rigorous theoretical approach based on energy and kinetic considerations through two different methods leading to the same result. The few simplifying assumptions made, especially the disregard of head losses, will have no quantitative or qualitative impact on the final result.

The study will continue with an intense experimental program involving six weirs tested in a specially designed facility. The ultimate objective is to confirm the validity of the derived theoretical relations or to correct them by the effects of an experimental correction factor if this proves necessary.

It is worth noting that the flow measurement method described in this paper must be applied to open channels conveying steady flow. The discharge to be measured is solely dependent on the upstream flow depth counted above the weir crest. Submerged flows whose discharge depends on both upstream and downstream levels are not considered in this study.

MATERIAL AND METHODS

Description of the device and the resulting flow

Fig. 1 gives a fairly precise overview of the device under consideration, inserted in a rectangular approach channel of width B and deep h_o, which conveys the flow rate Q sought. It is deliberately denoted " DEVICE' " to highlight its profile and its distinctive outline. The design is inspired by the Crump weir, in particular for the choice of upstream and downstream slopes. Preliminary tests have shown that slopes 1:2 and 1:5 of the upstream and downstream sloping faces, respectively, are the most appropriate values that ensure a stable and regular flow, without any separation on the weir crest or the downstream face, for a wide range of the discharge Q.

However, the involved cross sections are triangular throughout the current device, with a constant apex angle θ, unlike the Crump weir, which is based on rectangular cross sections. The choice of such a shape is motivated by the fact that triangular sections provide multiple advantages that are universally acknowledged since they ensure a more accurate flow measurement compared to the performance of other notch shapes, especially during low discharge measurements. Additionally, the accuracy is greater for the V-notch because it causes greater upstream depths than other notch shapes. The greater the upstream depth is, the greater the relative error of the depth measurement decreases, resulting in better accuracy in the calculation of the discharge. Moreover, even for shallow upstream depths, the measurement uncertainty is the same as that of greater depths since the triangular section offers a perfect geometrical similarity that is not found in the other section shapes.

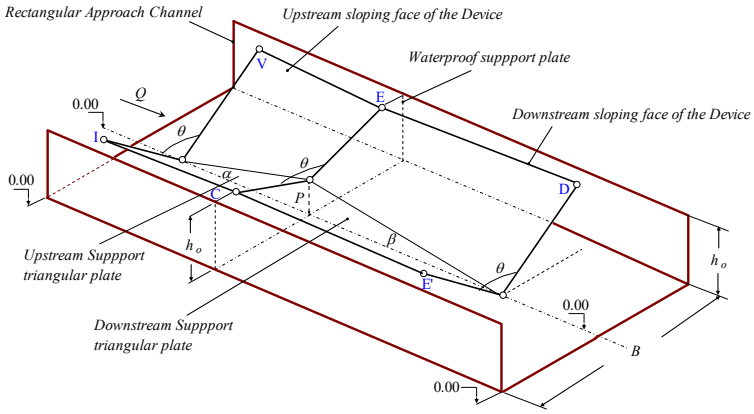

Figure 1: Perspective diagram of the device denoted DEVICE' inserted in a rectangular approach channel.

The device rests on a frame formed of waterproof plates, one placed vertically and perpendicular to the direction of flow, while the other two are placed vertically in the streamwise direction, in line with the longitudinal axis of the approach channel (Figs. 1 and 2). The longitudinal profile of these two plates is triangular. The one placed upstream supports the ascending face of the device with a slope of 1:2, while the one placed downstream supports the descending face of the device with a slope of 1:5. The vertical plate, which has a V-notch at its upper part, supports the weir crest of elevation P. Additionally, one may deduce from Fig. 2 that the maximal depth above the crest is

$$h_{\max} = (h_o - P)$$

As shown in Fig. 2, and Fig. 2.bis, the device is characterized by a triangular longitudinal profile, as the Bazin and Crump weirs are classified in this category.

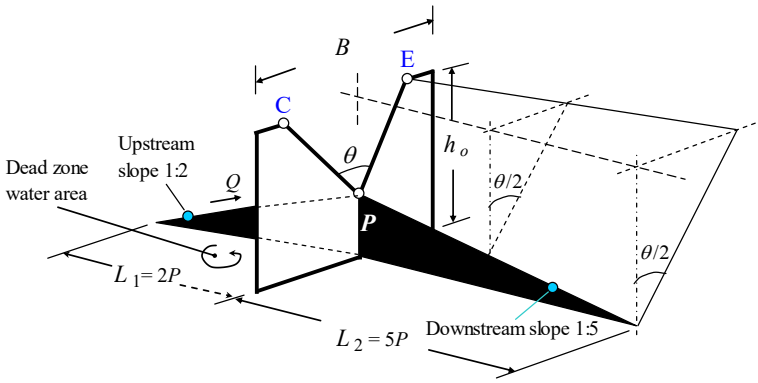

Figure 2: Perspective view of the device pedestal formed by the vertical waterproof support plate and the upstream and downstream support vertical shaped-triangular plates

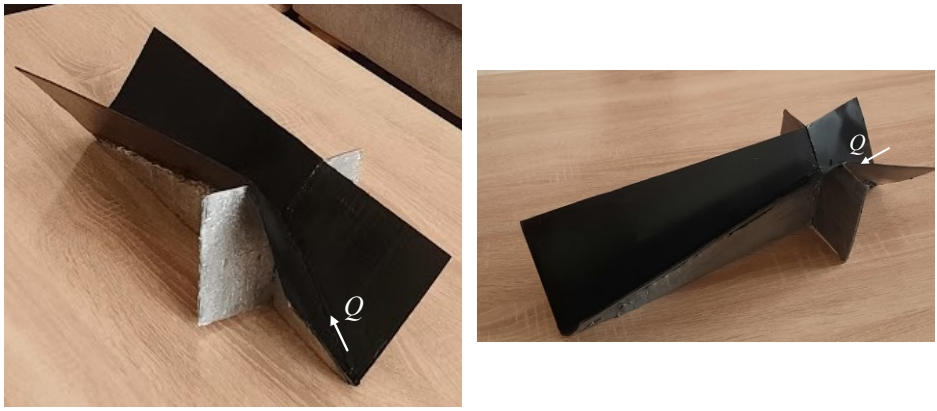

Figure 2bis: Photo views of the device under different perspective angles.

What has been described previously is an opportunity to qualitatively evolve the definition of weirs with a triangular longitudinal profile. It appears now that longitudinal profile weirs cannot be exclusively associated with rectangular cross-sections, as with Crump and Bazin-type weirs. A suitable definition could be based on the geometry of the cross-section of the device, in addition to the triangular shape of the longitudinal profile. The authors recommend designating, within the category of weirs with a triangular longitudinal profile, the C-rectangular weir, the B-rectangular weir, and the 2A-triangular weir as being the Crump (C) weir, Bazin (B) weir, and Achour-Amara (2A) weir, respectively. In the future, it would likely be that this definition will be completed by the X-parabolic weir or the Y-trapezoidal weir and even more, where X and Y designate the initiator, respectively,

It is worth noting that with such a design, the advocated device is of universal range since its use can be extended to any shape of the approach channel, including trapezoidal, semicircular, triangular, and parabolic. The main reason is that no lateral transition connecting the V-notched inlet of the device and the walls of the approach channel is made, which, therefore, does not affect either the discharge coefficient or the flow rate. Consequently, the relationships developed herein, governing both the discharge coefficient and the flow rate, remain valid regardless of the shape of the approach channel. The *sine qua non* condition for the user is compliance with the 1:2 and 1:5 slopes of the upstream and downstream faces of the device, respectively, so that the aforementioned relationships give reliable results. This requirement is recommended as a safety measure since no study carried out on the device attests that the upstream and downstream slopes do not influence the discharge coefficient. However, an earlier experimental study (Filippov and Brakeni, 2007) stated, with certainty, that no influence was observed on the flow rate through a Crump weir, tested with upstream and downstream slopes other than 1:2 and 1:5, respectively.

The simplest transition to achieve is a flat vertical plate perpendicular to the direction of flow, thus involving an abrupt transition. It would be used to close the space between the walls of the approach channel and the inlet V-notch of the device. It is essential to note that if the user adopts such a configuration, the theory presented herein as well as the resulting relationships governing the discharge coefficient and the flow rate are no longer valid. Another theory is appropriate in this case, involving the shape of the approach channel. If the device is inserted into a rectangular approach channel as in Fig. 1, in the presence of an abrupt transition, then the discharge coefficient will be influenced by the dimensionless parameter mh/B (Achour and Amara, 2022b), where $m = tg\,(\theta/2)$ and h is the upstream flow depth over the weir crest (Fig. 3).

Additionally, as seen in Figs. 1 and 2, between the vertical waterproof plate and the vertical shaped-triangular upstream plate, there is a space that will be occupied by water brought during flow; it is a dead zone water area that does not participate in the current flow. The water that enters this space will be prevented by the vertical watertight plate from passing to the downstream side, and the shaped-triangular vertical upstream plate will prevent the recirculation of water from left to right, and vice versa.

Fig. 3 shows the longitudinal profiles of the device and the resulting flow. This is a typical representation of a flow passing over a triangular longitudinal profile weir.

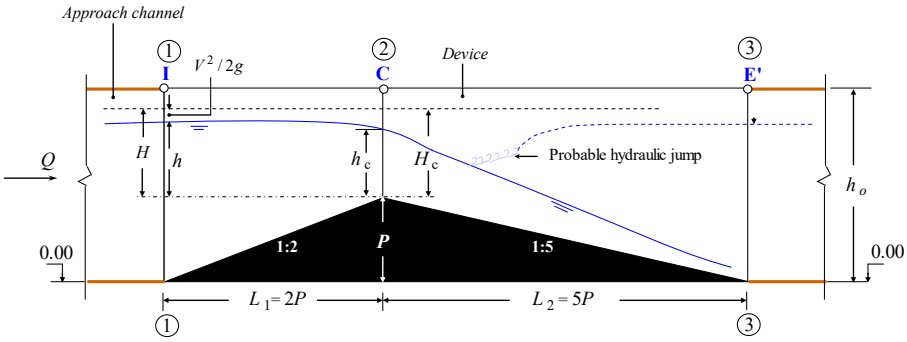

Figure 3: Schematic representation of the longitudinal profiles of both the device and the resulting flow

The putting in place of the weir of height P in the approach channel has a dual role since it creates a vertical contraction of the flow and causes the elevation of the upstream water level. The resulting change in the height of the upstream water level induces a subcritical state of the flow, characterized by an incident Froude number less than unity. Moreover, according to specialized literature (AFBLB, 1970), flow measurement in open channels requires the incident Froude number to be less than 0.50 to prevent the possible appearance of waves that could disturb the upstream h depth reading in measurement section 1 shown in Fig. 3.

Approaching the crest of the weir in the vicinity of section 2, where the cross-section is narrowed due to the effect of vertical contraction, the flow is accelerated to reach a supercritical state on the downstream face of the weir. The change in the state of the flow regime, from subcritical upstream to supercritical downstream, is accompanied by the appearance of a control section at the weir crest in section 2, where the critical depth is denoted h_c (Fig. 3). The presence of a control section is the *sine qua non* condition of the proper functioning of the weir as a measuring structure. As it is well known that there is a unique relationship between the flow rate Q and the critical depth h_c, the weir under consideration will be designed to serve as a flow measurement device provided that the Q-h relationship is determined. This is the main purpose of the study, however, emphasizing the fact that all the relationships that will be derived during this study are only valid in the case of a freely overflowed weir. For practical purposes, when weirs are used as flow measurement devices, it is strongly recommended that they operate every time under free-flow conditions.

The installation of the weir causes a reduction in the water area that passes from the initial water cross-section area $A = m(h+P)^2$ to the reduced cross-section, denoted A_R, such that $A_R = mh^2$ (Fig. 3). The ratio of these two quantities could define the vertical contraction rate (VCR), that is:

$$VCR = 1 - \frac{A_R}{A} = 1 - \frac{h^2}{(h+P)^2} \tag{1}$$

Eq. (1) can be rearranged as follows:

$$VCR = 1 - \frac{1}{\left(1+P^*\right)^2} = \frac{P^*\left(2+P^*\right)}{\left(1+P^*\right)^2} \tag{2}$$

where P^* is the relative weir height defined as follows:

$$P^* = \frac{P}{h} \tag{3}$$

P^* can be less than or equal to 1 or even greater than 1. For instance, when $P^* = 1/2$, Eq. (2) gives $VCR = 0.5555$, meaning that the section is reduced vertically by a rate of 55.55%, while $P^* = 1$ corresponds to $VCR = 0.75$ according to Eq. (2), meaning that the section undergoes a reduction rate of 75% in the vertical direction.

For comparative purposes, it is easy to show that in the case of rectangular sections that can be encountered in the case of Crump or Bazin weirs, VCR is equal to $P^*/(1+P^*)$. For $P^* = 1/2$, in the case of the Crump weir, for instance, it can be shown that $VCR = 1/3$, which means that the section undergoes a vertical reduction of 33.33%, while it was 55.55% for the case of the triangular section, as mentioned previously. For $P^* = 1$, one may show that $VCR = ½$ for the rectangular section, inducing a vertical contraction of 50%, while the previous calculation gave 75% in the case of the triangular section.

Based on the previous considerations, it can be concluded that the *VCR* in the case of a weir based on triangular cross-sections is larger than the *VCR* in the case of a weir formed by rectangular cross-sections for the same value of P^*. Calculations confirm this fact since, for the same relative weir height P^*, such as $P^* \neq 0$, the following ratio can be correctly written, which is less than unity regardless of the value of P^*:

$$\frac{VCR_{\text{Rectangular weir}}}{VCR_{\text{Triangularweir}}} = \frac{1+P^*}{2+P^*} \tag{4}$$

In the appropriate section of the paper, the important and even crucial role that the dimensionless parameter P^* plays in the relationships governing the coefficient C_d and the flow rate Q will be highlighted.

As mentioned above, the weir is assumed to be crossed by a critical flow of depth h_c. Since the involved cross-section is triangular, the critical depth h_c is expressed as follows (Chow, 1959; Henderson, 1966; Bos, 1976):

$$h_c = \left(\frac{2Q^2}{g\,m^2}\right)^{1/5} \tag{5}$$

where g is the acceleration due to gravity.

Additionally, neglecting insignificant head losses due to the short distances involved, Fig. 3 allows us to write the total head H as follows:

$$H = H_c \tag{6}$$

As the involved cross-section is triangular, Eq. (6) reduces to:

$$H = \frac{5}{4}h_c \tag{7}$$

The total head H includes the velocity head $V^2/(2g)$, where V denotes the mean flow velocity, assuming, however, that the kinetic energy correction factor is 1, as the involved state of the flow is turbulent. Thus, the total head H can be written as follows:

$$H = h + \frac{V^2}{2g} \tag{8}$$

Eq. (8) can be simply rewritten as follows:

$$H = \left(1 + \frac{V^2}{2gh}\right)h \tag{9}$$

Let us adopt the following reduced form for Eq. (9):

$$H = (1+\delta)h \tag{10}$$

where δ is a kinetic factor expressed as follows:

$$\delta = \frac{V^2}{2gh} = \left(\frac{V}{\sqrt{2gh}} \right)^2 \tag{11}$$

One may deduce from Eq. (11) that the kinetic factor δ is related to the ratio of the actual flow velocity V to the ideal flow velocity $\sqrt{2gh}$ given by Torricelli (Chow, 1959; Henderson, 1966, Bos, 1976).

Considering the general Eq. (10), it can be deduced that for the case of a rectangular cross section, the quantity $(1 + \delta)$ in parentheses is equal to 3/2 when the state of the flow is critical. Thus, the maximum value that δ can reach is ½, meaning that δ varies in the following range [0; ½] in the case of a rectangular cross-section. For the case of a triangular cross-section, as is the case of the considered weir, the quantity $(1 + \delta)$ in Eq. (10) is equal to 5/4 when the flow is critical, meaning that the maximum value of the kinetic factor δ is ¼. Thus, for a triangular cross-section, one may write that δ varies in the following range [0; ¼].

For the particular case where $\delta \to 0$, the approach flow velocity V is then insignificant, meaning that the total head H can be assimilated to the upstream depth h in accordance with Eq. (10).

It will be seen in an appropriate section of the paper that Eq. (9) along with Eq. (11) plays a momentous role in taking into account the approach flow velocity when deriving the theoretical relationship governing the discharge coefficient and hence that of the flow rate passing through the device.

On the other hand, as shown in section 3 (Fig. 3), by way of illustration, the level of the downstream flow can rise through the hydraulic jump, accidentally caused or deliberately created by the installation of a sluice gate or a sill further downstream. This study does not report the results obtained on the effects of submergence on both the discharge coefficient and the flow rate. The submergence transition, or the limit of the semimodularity, is not developed in detail herein, but it could be the subject of a future article.

Even if the downstream level rises, as shown in Fig. 3, the relationship governing the discharge coefficient, and hence the flow rate, that will be developed during this study remains valid as long as a supercritical flow slice is interspersed between the crest of the weir and the initial section of the hydraulic jump. This supercritical flow slice acts as a "sanitary cordon" that prevents any downstream disturbance from moving against the current and going up along the downstream face of the device to reach the upstream flow level.

Dimensional analysis and discharge coefficient dependency

One of the major advantages of dimensional analysis is its ability to reveal the influential dimensionless parameters of a given phenomenon and discard those of lesser interest. It is this advantage that this section wishes to exploit to highlight the parameters that influence the discharge coefficient C_d of the device, and hence the discharge Q. The dimensional analysis requires, as a first step, to enumerate the physical parameters involved in the raised problem. In the present case, one may identify the following influential parameters: the discharge Q, the upstream depth h, the apex angle θ, the acceleration due to gravity g, the density of the flowing liquid ρ, the dynamic viscosity μ of the liquid, and the surface tension σ. The discarded parameter is the width B of the rectangular approach channel because it is expected that this parameter will not influence the discharge coefficient C_d of the considered device.

The aforementioned parameters are interrelated by the following functional relationship:

$$f(Q,\rho,g,h,\mu,\sigma,\theta)=0 \tag{12}$$

The second step is to use the Vashy-Buckingham π theorem (Langhaar, 1951), along with Eq. (12), to derive the functional relationship that governs the discharge Q as a function of dimensionless parameters. The inferred final result is the following:

$$Q=g^{1/2}\,f(\theta)h^{5/2}\phi\left(\frac{\rho g^{1/2}h^{3/2}}{\mu},\frac{\rho g h^2}{\sigma},\frac{P}{h}\right) \tag{13}$$

Weir theory has shown that $f(\theta)=tg(\theta/2)=m$.

Referring to the standard form of the stage-discharge relationship of the triangular weir [1; 2], one may deduce from Eq. (13) the following relevant C_d functional relationship:

$$C_d=\phi\left(\frac{\rho g^{1/2}h^{3/2}}{\mu},\frac{\rho g h^2}{\sigma},\frac{P}{h}\right) \tag{14}$$

Thus, from Eq. (14), one may identify the first and the second quantities between the brackets corresponding to the Reynolds number R_e and the Weber number W_e, respectively (Lenz, 1943; Sarginson, 1972; 1973). Additionally, given the turbulent regime of the flow that prevailed in the device, the effect of the Reynolds number is not at all significant, as is the effect of the Weber number that appears only for low flow rates and reduced apex angles, i.e., for tightened triangular sections.

For these reasons, the effect of these two parameters on the discharge coefficient C_d cannot be envisaged given the experimental conditions adopted during the tests.

Thus, taking the previous considerations into account, Eq. (14) reduces to:

$$C_d=\lambda\left(\frac{P}{h}\right) \tag{15}$$

Eq. (15) can be rewritten simply as follows:

$$C_d = \lambda\left(P^*\right) \tag{16}$$

The λ functional relationship will be theoretically derived in the next sections through the judicious use of the energy equation, presented in dimensionless terms.

Discharge and discharge coefficient relationships

The kinetic factor approach

Combining Eqs. (5), (7), and (10) yields the following:

$$\left(\frac{2Q^2}{g\,m^2}\right)^{1/5} = \frac{4}{5}(1+\delta)h \tag{17}$$

It is easy to deduce from Eq. (17) what follows:

$$Q^2 = \frac{1}{2}\left(\frac{4}{5}\right)^5 m^2 g(1+\delta)^5 h^5 \tag{18}$$

On the other hand, using continuity equation $V = Q/A$, Eq. (11) becomes:

$$\delta = \frac{Q^2}{2ghm^2(h+P)^4} \tag{19}$$

Introducing the relative weir height P^*expressed by Eq. (3), Eq. (19) reduces to:

$$\delta = \frac{Q^2}{2gh^5 m^2\left(1+P^*\right)^4} \tag{20}$$

Elimination Q^2 between Eqs. (18) and (20) and operating some arrangements results in the following:

$$\delta = \frac{1}{4}\left(\frac{4}{5}\right)^5 \frac{(1+\delta)^5}{\left(1+P^*\right)^4} \tag{21}$$

One may deduce from Eq. (21) that the kinetic factor δ is fully controlled by the relative weir height P^*, which is the only influential parameter. However, Eq. (21) is implicit in δ, which must be solved by an iterative process, provided that the value of $P^*$is given.

Let us denote C_o as the following constant:

$$C_o = 4\left(\frac{5}{4}\right)^5 \tag{22}$$

Thus, Eq. (21) can be rewritten as follows:

$$\delta = \frac{(1+\delta)^5}{C_o\left(1+P^*\right)^4} \tag{23}$$

It has been shown previously that the kinetic factor δ varies in the range [0; ¼] in the case of a triangular cross-section, but it would be useful to refine this range of variation for the practical values of P^* in accordance with Eq. (23). Calculations, based on an iterative procedure operated on the implicit Eq. (23), showed that when P^* varies in the range [0.10; 2], the kinetic factor delta varies in the range [0.083587; 0.0010165]. It can thus be concluded that the kinetic factor δ remains substantially below its greatest value ¼, which does not mean that δ can be neglected because it is not δ that intervenes in Eq. (18), which governs the flow rate Q, but it is $(1+\delta)^{5/2}$ that is the influential quantity. Calculations show that the quantity $(1+\delta)^{5/2}$ varies in the range [1.2222; 1.0025] when P^* varies in the range [0.10; 2]. This result indicates that significant errors could affect the calculation of the flow rate Q if the kinetic factor δ were to be neglected. For illustrative purposes, given the following practical value of the relative weir height P^* = 0.30, the calculation shows that $(1+\delta)^{5/2}$ = 1.08687. This amounts to saying that if, in this case, the kinetic factor δ were neglected, then the calculation of the flow rate Q would be affected by a deviation of approximately 8.7%, which could have undesirable consequences in certain practical cases that require better accuracy.

Thus, since $\delta << 1$, as the result of a second-order Taylor series expansion (Canuto and Tabacco, 2015), it is relevant to write the following:

$$(1+\delta)^5 \approx 1+5\delta+10\delta^2 \tag{24}$$

Inserting Eq. (24) into Eq. (23) and rearranging the results in the following quadratic equation in δ:

$$\delta^2 - \frac{1}{10}\left[C_o\left(1+P^*\right)^4 - 5\right]\delta + \frac{1}{10} = 0 \tag{25}$$

The real root of Eq. (25) that satisfies the condition $\delta < 1$ is such that:

$$\delta = \psi - \sqrt{\psi^2 - 0.1} \tag{26}$$

where ψ is expressed as follows:

$$\psi = \frac{1}{20}\left[C_o\left(1+P^*\right)^4 - 5\right] \tag{27}$$

Table 1 gives the deviations caused by the approximate Eq. (26), along with Eq. (27), in comparison with Eq. (23) in the practical wide range $0.10 \le P^* \le 2$.

Note that the maximum deviation value of 0.65% given by Table 1 is obtained for the low-value P^* = 0.10 of the relative weir height, which is rarely a commonly used relative

weir height. The maximum deviation drops to 0.32% for $P^* \geq 0.14$. These figures confirm the great accuracy of the approximate Eq. (26) along with Eq. (27).

Table 1: Deviations in the values of δ given by exact and approximate Eqs. (23) and (26), respectively

Range of P^*	Deviation (%) between Eqs. (23) and (26)		
	Minimum	Maximum	Average
$0.10 \leq P^* \leq 2$	0.00	0.65	0.033

It is well known that the standard form of the stage-discharge relationship governing triangular weirs is as follows (Henderson, 1966; Bos, 1976):

$$Q = \frac{8}{15} C_d \, m \sqrt{2g} \; h^{5/2} \tag{28}$$

Comparing Eqs. (18) and (28) results in the following exact discharge coefficient relationship for the current device:

$$C_d = \frac{15}{8\sqrt{C_o}} \left(1+\delta\right)^{5/2} \tag{29}$$

Inserting Eq. (26) into Eq. (29) results in the following explicit approximate discharge-coefficient relationship of the device under consideration:

$$C_d = \frac{15}{8\sqrt{C_o}} \left(1+\psi-\sqrt{\psi^2-0.1}\right)^{5/2} \tag{30}$$

If the user is longing to compute the exact value of the discharge coefficient C_d of the device, for a given installation, then the simultaneous use of Eqs. (23) and (29) are needed, bearing in mind the drawbacks that the iterative calculation could entail. However, the authors recommend the simplest approach, which consists of the use of explicit Eq. (30) along with Eq. (27). The maximum deviation of 0.65% committed in the calculation of the kinetic factor δ as indicated previously, for $P^* \geq 0.10$, induces a maximum deviation of only 0.125% in the discharge coefficient C_d when using Eq. (30). The maximum deviation drops to less than 0.08% for $P^* \geq 0.12$. Additionally, the same maximum deviation results during the flow rate Q computation according to Eq. (28).

For the particular case corresponding to large values of the relative height P^* of the weir, which could be translated mathematically by $P^* \rightarrow \infty$, Eq. (27) also implies large values of ψ, such as $\psi >> 0.1$. Consequently, Eq. (30) reduces to:

$$C_d = \frac{15}{8\sqrt{C_o}} \left(1+\psi-\sqrt{\psi^2-0.1}\right)^{5/2} \approx \frac{15}{8\sqrt{C_o}} \left(1+\psi-\psi\right)^{5/2} = \frac{15}{8\sqrt{C_o}} \approx 0.5366 \tag{30a}$$

This particular discharge coefficient value corresponds exactly to that given by the theoretical formula derived by the authors for a triangular notch weir, provided $P^* \to \infty$ (Achour and Amara, 2021). This result could have been simply deduced from Eq. (29) by writing that the kinetic factor δ is such that $\delta \to 0$ since $P^* \to \infty$.

Energy equation approach

With the help of the continuity equation, Eq. (8) can be written as follows:

$$H = h + \frac{Q^2}{2g\,m^2\left(h+P\right)^4} \tag{31}$$

Dividing both sides of Eq. (31) by h_c and considering both Eqs. (3) and (5) results in the following:

$$H^* = h^* + \frac{1}{4}h^{*-4}(1+P^*)^{-4} \tag{32}$$

Eq. (32) is the energy equation presented in dimensionless terms, where $H^* = H/h_c$ and $h^* = h/h_c$. The relative depth h^* is greater than 1 since $h > h_c$, as shown in Fig. 3. Additionally, Eq. (7) reveals that H^* = constant = 5/4. Introducing this result into Eq. (32) and rearranging yields the following quintic equation in h^*:

$$h^{*5} - \frac{5}{4}h^{*4} + \frac{1}{4}\left(1+P^*\right)^{-4} = 0 \tag{33}$$

For $P^* \to 0$, corresponding to small elevations P of the weir crest or to large depths h, Eq. (33) is satisfied only for $h^* = 1$, meaning that the flow reaches the critical state. For $P^* \to \infty$, corresponding to large elevations P of the weir crest or to shallow depths h, one may write $H^* = h^* = 5/4$ according to Eqs. (32) and (33). This means that the weir is freely overflowed under critical flow conditions, with a total head H that can be assimilated to the depth h over the weir since the kinetic factor is $\delta \to 0$ in accordance with Eq. (23).

On the other hand, writing $h_c = h/h^*$ in Eq. (5) results in the following discharge Q relationship:

$$Q = \frac{1}{2}\sqrt{2g}\,m\,h^{*-5/2}h^{5/2} \tag{34}$$

Comparing Eqs. (28) and (34) results in the following exact discharge coefficient C_d relationship of the device, depending solely on the relative depth h^*:

$$C_d = \frac{15}{16}h^{*-5/2} \tag{35}$$

Although derived from two different methods, Eqs. (30) and (35) nevertheless give the same result. For the given value of P^*, Eq. (35) along with Eq. (33) gives the exact discharge coefficient C_d of the device. However, Eq. (33) is implicit in h^*, requiring an

iterative procedure to find its solutions. Trial and error is the most well-known method of solving implicit equations. However, although it is simple and understandable, trial and error is not a very elegant way to seek a solution to an implicit equation. To avoid the drawbacks resulting from this method of resolution, the authors recommend the use of the following explicit approximate relationship for h^*, inspired by the theoretical considerations developed in the previous section:

$$h^*_{app} = \frac{5}{4}\left(1 + \psi - \sqrt{\psi^2 - 0.1}\right)^{-1} \tag{36}$$

where the subscript "app" denotes "Approximate". In Eq. (36), the parameter ψ is also governed by Eq. (27) developed in the previous section. Intense calculations were able to conclude that the maximum deviation caused by the approximate Eq. (36) along with Eq. (27) in the h^* computation is only 0.05% for any value of P^* such that $P^* \geq 0.10$, thus encompassing all practical cases. Consequently, according to Eq. (35), the maximum deviation caused in the discharge coefficient C_d calculation is 0.05% x (5/2) = 0.125%, bearing in mind that it is the same maximum deviation affecting C_d computation when using Eq. (30).

Incident Froude number

Let us denote by F the incident Froude number characterizing the flow in section 1 (Fig. 3) in the triangular measuring section at the inlet of the device. The Froude number F is relevant in the current case since the flow occurring in the corresponding section is characterized by a predominance of gravitational forces. Inertial forces also exist, but they are not as preponderant. As a result, the flow is subcritical, inducing an incident Froude number F less than 1. The subcritical flow in the considered section 1 of Fig. 3 is controlled by the presence of the weir, which can be likened to a local disturbance. Therefore, it is expected that the incident Froude number F is closely related to the characteristics of the weir, particularly the relative height P^*.

T is assumed to be the top width at the water surface of the flow in section 1 (Fig. 3), where the depth is $(h + P)$ corresponding to the water area $A = m(h+P)^2$. It is easy to show that the top width T is such that $T = 2m(h+P)$. The Froude number is typically expressed in the following form (Chow, 1959; Henderson, 1966; Bos, 1976):

$$F^2 = \frac{Q^2 T}{g A^3} \tag{37}$$

Thus, for the current case, Eq. (37) becomes the following:

$$F^2 = \frac{Q^2\, 2m(h+P)}{g\left[m(h+P)^2\right]^3} \tag{38}$$

After simplifications and rearrangements, Eq. (38) reduces to the following:

$$F^2 = \frac{2Q^2}{g\,m^2 h^5 (1+P^*)^5} \tag{39}$$

Considering Eq. (5) in which h_c is replaced by h/h^*, Eq. (39) is reduced to the following:

$$F^2 = \frac{1}{h^{*5}(1+P^*)^5} \tag{40}$$

That is,

$$F = \left[h^*\left(1+P^*\right)\right]^{-5/2} \tag{41}$$

As expected, Eq. (41) shows that the incident Froude number F is exclusively controlled by the relative weir height P^*, bearing in mind that h^* depends solely on P^* according to Eq. (33). As this equation is implicit, it is recommended to use the approximate relationship (36) that governs $h^*(P^*)$. Therefore, Eq. (41) reduces to the following:

$$F = \frac{2}{\sqrt{C_o}}\left(\frac{1+\psi-\sqrt{\psi^2-0.1}}{1+P^*}\right)^{5/2} \tag{42}$$

It is useful to remember that parameter ψ is governed by Eq. (27) as solely dependent on P^*. Additionally, Eq. (42) is applicable as long as P^* is greater than or equal to 0.10. According to Eq. (41), the maximum deviation caused in the calculation of the incident Froude number F is 2.5 times the maximum deviation caused in the calculation of $h^*$when using approximate Eq. (36), i.e., 2.5 x 0.05% = 0.125%.

In agreement with the calculations derived from Eq. (42), for the smallest value $P^* = 0.10$ considered herein, the incident Froude number is such that $F = 0.55$. This is a value slightly higher than the upper limit value recommended by the specialized literature, i.e., $F = 0.50$, to prevent the formation of waves that could disturb the accurate upstream depth reading.

Experimental validation

This part of the study seeks to provide more definitive conclusions about the reliability of the theoretical relationships presented in the previous sections, particularly the discharge coefficient relationship expressed by Eq. (30) or Eq. (35). By analyzing experimental data collected on devices with various geometrical characteristics, users may corroborate the reliability and accuracy of the derived theoretical relationships. In the case where experimental data are not entirely consistent with the theoretical results, the latter require corrections to conform to actual observations. This is the approach adopted by the authors during this part of the study.

Given the major importance of collecting quality data in the field of flow measurement, the influential parameters were measured using irreprovable precision devices. This is mainly the case for the measured flow rate Q, which was deduced from the average between the discharge value read on an ultrasonic flow meter and that of the discharge read on a magnetic flow meter; both devices have been carefully calibrated. The absolute error caused by this procedure on the estimation of the flow rate Q was ± 0.1 l/s. The other influential parameter is the upstream depth h, which was measured using a double-precision Vernier point gauge and graduated to 1/10th, implying an absolute error of 0.02 mm in h depth reading (Achour and Amara, 2022b).

To obtain a representative measurement sample, allowing reliable analysis, six devices were designed and subjected to an intense experimental program. The devices were tested in a specially equipped installation consisting of a canal supply basin upstream and a water recovery basin downstream (Fig. 4). The supply basin is filled using a pump that draws water from an underground tank. The pump is fitted with an adjustment valve that allows the test channel to be supplied with a given flow rate Q. The test channel into which the devices were inserted, as represented in Fig. 1, was of a rectangular cross-section with a width B = 0.40 m, depth 0.485 m, and length 4.00 m sufficient to ensure tests of the longest designed device of 1.75 m length. Additionally, the upstream and downstream slopes of the six designed devices were chosen as recommended for the Crump weir, i.e., 1:2 and 1:5, respectively. The characteristics of the six devices designed and tested are grouped in Table 2.

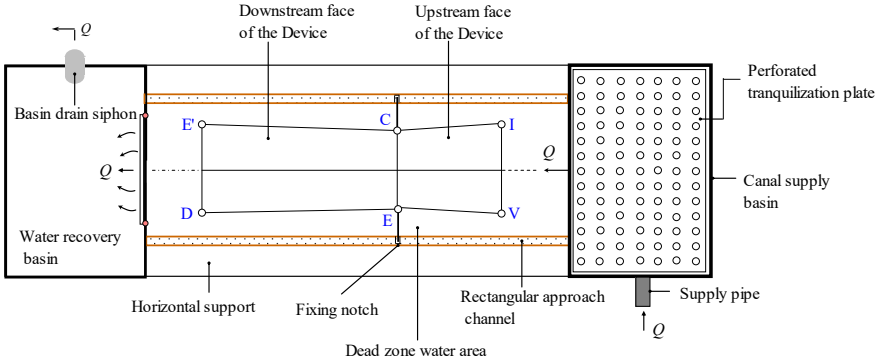

Figure 4: Plan view of the installation used during testing of the devices

Table 2: Characteristics of the tested devices. Same notation as in Figs. 1, 2, and 3

Device	P (m)	θ (°)	L_1 (m)	L_2 (m)	$L_1 + L_2$ (m)
1	0.10	32	0.20	0.50	0.70
2	0.12	35	0.24	0.60	0.84
3	0.15	38	0.30	0.75	1.05
4	0.18	41	0.36	0.90	1.26
5	0.21	42.5	0.42	1.05	1.47
6	0.25	44.3	0.50	1.25	1.75

The installation described in Fig. 4, as well as its equipment, allowed us to vary the discharge Q in the wide range 0.127 l/s ≤ Q_{Exp} ≤ 27.18 l/s by manipulating the adjustment valve incorporated in the pump, while the upstream depth h_{Exp} was varied in the range 3.85 cm ≤ h ≤ 33.26 cm. The subscript "*Exp*" denotes "Experimental". A total of 1347 values (Q_{Exp}; h_{Exp}) were experimentally collected during the testing of the six designed devices. Details of the experimental conditions for each of the six tested devices are given in Table 3.

Table 3: Range of the influential parameters used during the testing devices

Device	Number of measurements	Range of the discharge Q_{Exp} (l/s)	Range of upstream depths h_{Exp} (cm)	Range of $P^*_{Exp} = P/h_{Exp}$
1	95	[0.211; 23.48]	[5.07; 32.36]	[0.309; 1.972]
2	171	[0.173; 27.18]	[4.51; 33.21]	[0.361; 2.660]
3	263	[0.127; 22.07]	[3.85; 29.78]	[0.503; 3.896]
4	306	[0.187; 21.10]	[4.35; 28.45]	[0.632; 4.138]
5	270	[0.218; 15.63]	[4.55; 25.01]	[1.000; 5.494]
6	242	[0.212; 10.55]	[4.42; 21.02]	[1.189; 5.656]

For a given tested device, each of the pairs (Q_{Exp}; h_{Exp}) obtained allows us to calculate the experimental discharge coefficient according to Eq. (28), such as:

$$C_{d,\,Exp} = \frac{15}{8}\frac{Q_{Exp}}{m\sqrt{2g}\,h_{Exp}^{5/2}} \tag{28a}$$

For each of the six tested devices, the experimental discharge coefficient $C_{d,Exp}$ is compared to the theoretical discharge coefficient $C_{d,Th}$ given by Eq. (30), along with Eq. (27), for the given value of the experimental relative weir height P^*_{Exp}. The subscript "*Th*" denotes "Theoretical". This comparison is highlighted in Fig. 6 (a) to (f), showing the theoretical and experimental variation in the discharge coefficient C_d as a function of P^* for each device.

Figs. 5a to 5f show good agreement between the theoretical and experimental discharge coefficients, confirming the validity of Eq. (30), provided the P^* range of validity, given in Table 3, is respected. Therefore, Eq. (30), along with Eq. (27), is an excellent model for predicting the discharge coefficient of the device under consideration, and hence, the discharge Q sought using Eq. (28), with great confidence.

To confirm this result, the maximum, minimum and average deviations between the theoretical and experimental values of the discharge coefficient are grouped together in Table 4 for each device. It can be observed with satisfaction that the maximum deviations are very satisfactory, which proves that the values of the discharge coefficient predicted by Eq. (30) are very close to the observed values.

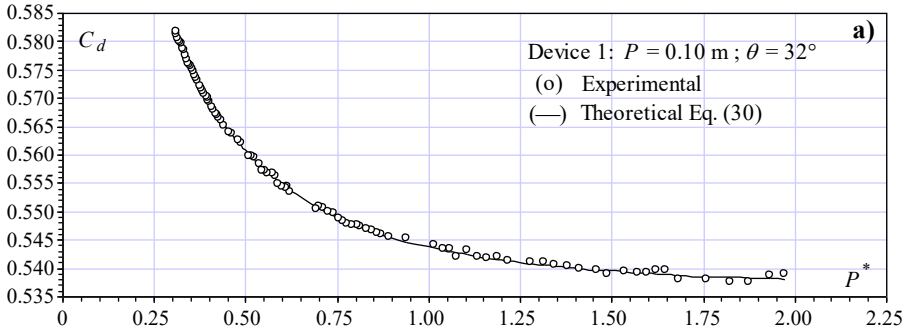
C_d
a)
Device 1: P = 0.10 m ; θ = 32°
(o) Experimental
(—) Theoretical Eq. (30)
P^*
0.585
0.580
0.575
0.570
0.565
0.560
0.555
0.550
0.545
0.540
0.535
0
0.25
0.50
0.75
1.00
1.25
1.50
1.75
2.00
2.25

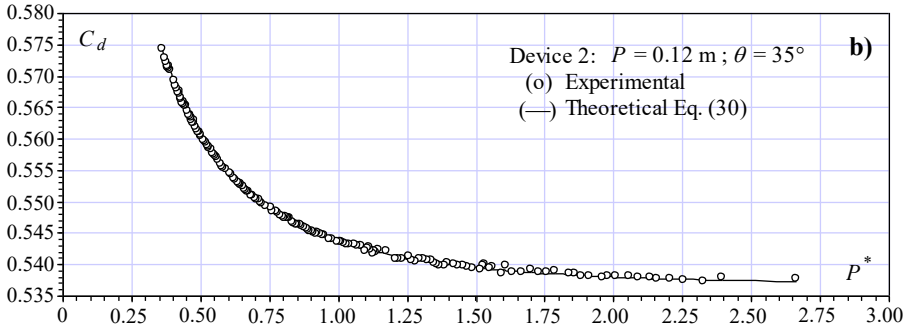
C_d
b)
Device 2: P = 0.12 m ; θ = 35°
(o) Experimental
(—) Theoretical Eq. (30)
P^*
0.580
0.575
0.570
0.565
0.560
0.555
0.550
0.545
0.540
0.535
0
0.25
0.50
0.75
1.00
1.25
1.50
1.75
2.00
2.25
2.50
2.75
3.00

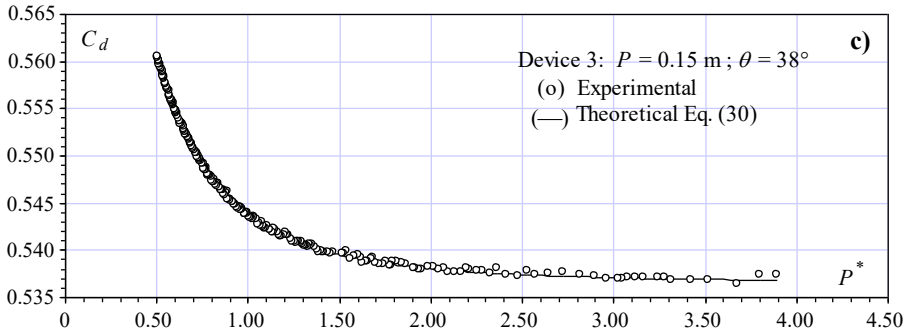
C_d
c)
Device 3: P = 0.15 m ; θ = 38°
(o) Experimental
(—) Theoretical Eq. (30)
P^*
0.565
0.560
0.555
0.550
0.545
0.540
0.535
0
0.50
1.00
1.50
2.00
2.50
3.00
3.50
4.00
4.50

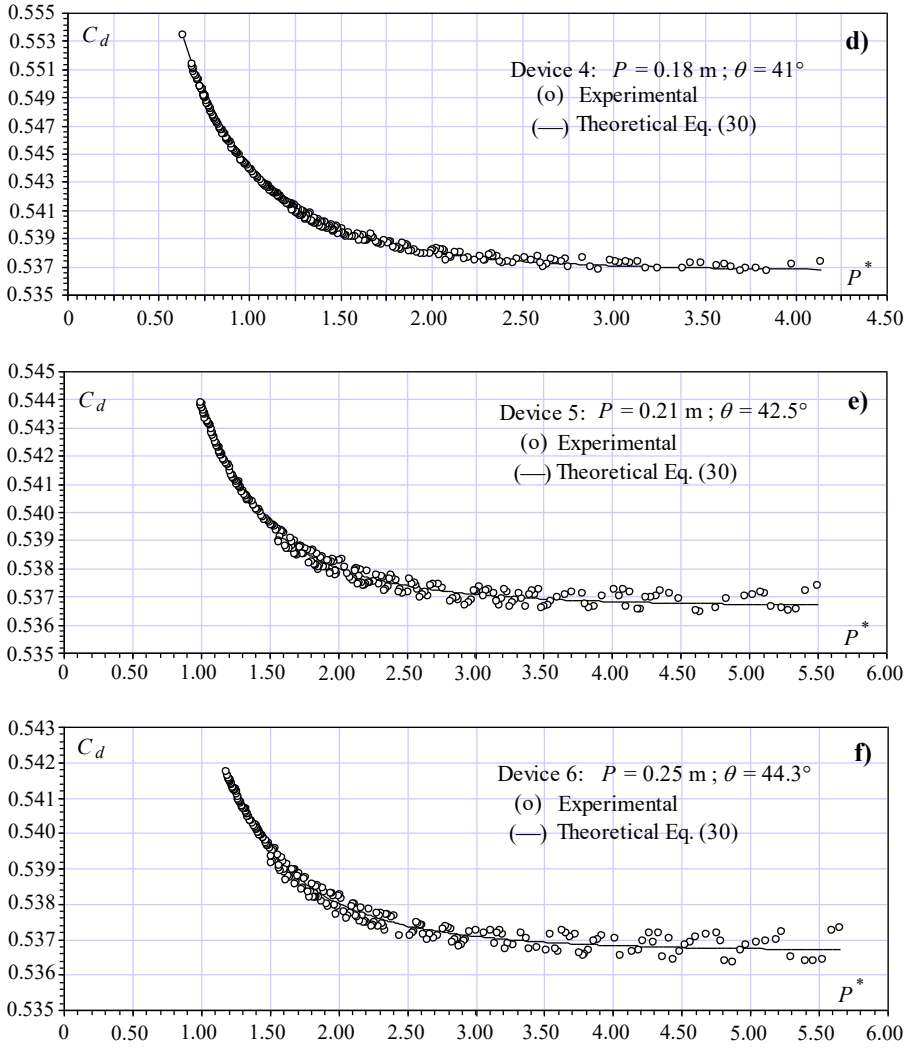

Figure 5: Variation in the theoretical and experimental discharge coefficients C_d against the relative weir height P^*

Table 4: Deviations $\Delta C_d / C_d$ between theoretical Eq. (30) and observations for each of the tested devices

Device	$\Delta C_d / C_d$ (%)		
	Minimum	**Maximum**	**Average**
1	0.0017	0.150	0.045
2	0.0017	0.147	0.032
3	0.0015	0.112	0.037
4	0.0012	0.101	0.033
5	0.0012	0.121	0.034
6	0.0012	0.114	0.033

CONCLUSION

The 2A triangular weir is a structure intended for flow measurement in open channels. It can be classified as a weir with a triangular longitudinal profile, such as the Crump and Bazin weirs. The difference is that the new structure is formed of triangular cross-sections, the advantages of which are widely known, recognized, and universally appreciated, while those of the Crump- and Bazin-type weirs are rectangular, which are known to be of least practical interest.

The 2A weir adopts the same upstream and downstream face slopes as the Crump weir, i.e., 1:2 and 1:5, respectively, because experience has shown that these slopes do not cause any separation of the flow over the weir crest and along the downstream face.

The main purpose of the study was to derive the theoretical discharge coefficient C_d relationship based on rigorous theoretical considerations. That is why the authors called upon the energetic and kinetic principles through two methods that gave the same result. The obtained discharge coefficient relationship thus showed that the relative weir height P^* was the only influential parameter, as predicted by the dimensional analysis.

Thanks to the design that characterizes the structure, the theoretical discharge coefficient relationship remains unchanged regardless of the shape of the approach channel; the 2A triangular weir is thus a universal range structure.

A total of 1347 measurement points of the *Q-h* couple were experimentally collected on six weirs with different geometric characteristics. The objective of this approach was either to validate the proposed theoretical relationships or to correct them by the effect of an experimental adjustment factor. The in-depth analysis of the observations confirmed the reliability and accuracy of both the discharge coefficient relationship and the stage-discharge relationship since the maximum deviation caused is 0.15% over a wide range of the influential parameter P^*.

Declaration of competing interest

The authors declare that they have no known competing financial interests or personal relationships that could have appeared to influence the work reported in this paper.

REFERENCES

ACHOUR B., AMARA L. (2021). Discharge coefficient for a triangular notch weir theory and experimental analysis, Larhyss Journal, No 46, pp. 7–19.

ACHOUR B., AMARA L. (2022a). Flow measurement using a triangular broad–crested weir–theory and experimental validation, Flow Measurement and Instrumentation, Vol. 83, Paper 102088.

ACHOUR B., AMARA L. (2022b). Discharge coefficient relationship for the sharp-edged width constriction, new theory and experiment, Flow Measurement and. Instrumentation, Vol. 88, Paper 102269.

AFBLB. Agence Financière du Bassin Loire et Bretagne. (1970). Book of special requirements for the production and approval of devices for measuring the flow of effluents. (In French)

BAZIN H. (1898). In: New Experiments on Weir Flow, Ed. Dunod, Paris, France. (In French)

BOITEN W., PITLO R.H. (1982) The V-shaped broad-crested weir, Journal of Irrigation and Drainage Division, Vol. 108, Issue 2, pp. 142–160.

BOS M.G. (1976). Discharge Measurement Structures, Laboratorium Voor Hydraulica Aan Afvoerhydrologie, Landbouwhogeschool, Wageningen, the Netherlands.

BOS M.G. (1989). Discharge Measurement Structures, third ed., Publication 20, Int. Institute for Land Reclamation and Improvement, Wageningen, the Netherlands.

CANUTO C., TABACCO A. (2015). Mathematical Analysis I, 2nd Edition, Springer, Part of the Book series UNITEXT, Vol. 84.

CHOW V.T. (1959). Open-Channel Hydraulics, McGraw Hill, New York, USA.

DE COURSEY D.E., BLANCHARD B.J. (1970). Flow analysis over large triangular weir, Proceedings ASCE, Journal of Hydraulic Division, Vol. 96, (HY7), pp. 1435–1454.

FILIPPOV Y.G., BRAKENI A. (2007). Use of weirs with sill of triangular profile for measurement of discharges of water in open streams and conduits," in: Problems of Stable Development of Reclamation and Rational Resource Management: Proceedings International. Science-Practice, Jubilee Conference (Kostyakov Session), Izd. VNIIA, Moscow, pp. 338-343. (In Russian)

HAGER W.H. (1986). Discharge Measurement Structures, Communication 1, Department of Civil Engineering, Federal Polytechnic School of Lausanne, Switzerland. (In French)

HENDERSON F.M. (1966). Open Channel Flow, McMillan Company, New York, N.Y, USA.

KINDSVATER C.E., CARTER R.W. (1957). Discharge characteristics of rectangular thin-plate weirs, Proceedings ASCE, Journal of Hydraulic Division, Vol. 83, (HY6), 1453/1–6.

KULIN G., COMPTON P.R. (1975). A Guide to Methods and Standards for the Measurement of Water Flow, Special Publication 421, U.S Department of Commerce, National Bureau of Standards, Washington, USA.

LANGHAAR H.L. (1951). Dimensional Analysis and Theory of Models, John Wiley and Son Ltd, 1st Edition, USA.

LENZ A.T. (1943). Viscosity and surface tension effects on V-notch coefficients, Transactions ASCE, Vol. 108, pp. 759–781.

NICOSIA A., FERRO V. (2022). A new approach for deducing the stage-discharge relationship of a triangular broad-crested device, Flow Measurement and Instrumentation, Vol. 85, Paper 102160.

SARGINSON E.J. (1972). The influence of surface tension on weir flow, Journal of Hydraulic Research, Vol. 10, Issue 4, pp. 431–446.

SARGINSON E.J. (1973). The influence of surface tension on weir flow, Journal of Hydraulic Research, Vol. 11, Issue 3, pp. 299–306.

SHEN J. (1981). Discharge Characteristics of Triangular-notch Thin-plate Weirs, Geological Survey Water Supply, Paper 1617-B, Washington, USA.

SIA (1926). in: Contribution to the Study of Gauging Methods, Bureau Wasserfoschung, Bull. 18, Schw, Bern. (In French)

THOMSON J. (1861). On experiments on the measurement of water by triangular notches in weir boards, The British Association for the Advancement of Science, Annual report, p. 151.

USBR (1997). Water Measurement Manual, U.S. Department of the Interior, Bureau of Reclamation, 3th Ed.

ZUIKOV A.L. (2017). Hydraulics of the classical Crump weir water gauge, Power Technology and Engineering, Vol. 50, Issue 6, pp. 50-59.